

ORIGINAL RESEARCH

Radius exponent in elastic and rigid arterial models optimized by the least energy principle

Yoshihiro Nakamura¹ & Shoichi Awa²

¹ Department of Pediatrics, Graduate School of Medicine, University of Tokyo, 7-3-1 Hongo, Bunkyo-ku, Tokyo, 113-8655, Japan

² (Formerly) Department of Pediatrics, Kyorin University School of Medicine, 6-20-2 Shinkawa, Mitaka city, Tokyo, 181-8611, Japan

Keywords

Bernoulli's equation, Murray's law, optimality principle, Poiseuille's law, Reynolds number.

Correspondence

Yoshihiro Nakamura, Department of Pediatrics, Graduate School of Medicine, University of Tokyo, 7-3-1 Hongo, Bunkyo-ku, Tokyo 113-8655, Japan.
Tel.: +81-3-3815-5411 ex. 33456
Fax: +81-3-3816-4108
E-mail: yonakamura-tyk@umin.ac.jp

Funding Information

None declared.

Received: 10 October 2013; Revised: 17 January 2014; Accepted: 20 January 2014

doi: 10.1002/phy2.236

Physiol Rep, 2 (2), 2014, e00236,
doi: 10.1002/phy2.236

Abstract

It was analyzed in normal physiological arteries whether the least energy principle would suffice to account for the radius exponent x . The mammalian arterial system was modeled as two types, the elastic or the rigid, to which Bernoulli's and Hagen-Poiseuille's equations were applied, respectively. We minimized the total energy function E , which was defined as the sum of kinetic, pressure, metabolic and thermal energies, and loss of each per unit time in a single artery transporting viscous incompressible blood. Assuming a scaling exponent α between the vessel radius (r) and length (l) to be 1.0, x resulted in 2.33 in the elastic model. The rigid model provided a continuously changing x from 2.33 to 3.0, which corresponded to Uylings' and Murray's theories, respectively, through a function combining Reynolds number with a proportional coefficient of the $l - r$ relationship. These results were expanded to an asymmetric arterial fractal tree with the blood flow preservation rule. While x in the optimal elastic model accounted for around 2.3 in proximal systemic ($r > 1$ mm) and whole pulmonary arteries ($r \geq 0.004$ mm), optimal x in the rigid model explained 2.7 in elastic-muscular ($0.1 < r \leq 1$ mm) and 3.0 in peripheral resistive systemic arteries ($0.004 \leq r \leq 0.1$ mm), in agreement with data obtained from angiographic, cast-morphometric, and in vivo experimental studies in the literature. The least energy principle on the total energy basis provides an alternate concept of optimality relating to mammalian arterial fractal dimensions under $\alpha = 1.0$.

Introduction

Mean aortic blood pressure falls only 2% from the ascending aorta to small arteries whose inner radius (r) narrows to ~ 1 mm (Struijker-Boudier 2009) (or ~ 2.5 mm, Nichols et al. 2011) in the human systemic circulation (Nichols et al. 2011). The normal pulmonary arterial circulation shares 50% (Brody et al. 1968; Bhattacharya and Staub 1980; Michel et al. 1985) of the whole mean transpulmonary pressure gradient, which is as low as 6–7 mmHg in humans (Fowler 1980; Kovacs et al. 2009; Nakamura et al. 2011). The common factor in these two small pressure-losing systems lies largely in the elasticity of its arterial wall (Patel et al. 1960; Learoyd 1966; Gow and Taylor 1968; Milnor 1982; Zhuang et al. 1983; Al-Tinawi et al. 1991; Gan and Yen 1994; Dawson et al. 1999; Nichols et al. 2011). The sufficient elasticity and

resultant large distensibility in proximal systemic arteries are due to the large ratio of constituent elastin over collagen and the thin smooth muscle layer (Struijker-Boudier 2009; Nichols et al. 2011). On the other hand, the pulmonary arterial wall is much thinner, less-or-non muscularized, and more distensible than its systemic counterpart (Patel et al. 1960; Gow and Taylor 1968; Milnor 1982; Al-Tinawi et al. 1991; Guyton 1991; Dawson et al. 1999; Nichols et al. 2011). Thus, even though peripheral pulmonary arteries of $r \leq 0.1$ mm comprise the most resistive in the pulmonary circulation (Bhattacharya and Staub 1980; Michel et al. 1985), the mean pressure gradient through them amounts to only 2.8 mmHg, as estimated in controls of our clinical data (Nakamura et al. 2011).

By contrast, as much as 60% of mean aortic blood pressure is lost in peripheral systemic resistive arteries ($0.004 \leq r \leq 0.1$ mm) (Nichols et al. 2011). A much smal-

ler elastin/collagen ratio in more peripheral systemic arteries renders their wall a lot stiffer (Learoyd 1966; Gow and Taylor 1968; Struijker-Boudier 2009; Nichols et al. 2011). Furthermore, adding a thick smooth muscle layer to this already stiffer wall property makes the change in the radius in response to internal pulsatile pressure alteration extremely small in systemic arterioles (Meyer et al. 1988; Nichols et al. 2011).

Some histologists, however, advocate another intermediate category of systemic arteries around $0.1 < r_s \leq 1$ mm (Struijker-Boudier 2009) (or ≤ 2.5 mm, Nichols et al. 2011), where the pressure gradient comprises 8% of mean aortic pressure in humans (Nichols et al. 2011). They describe it as elastic-muscular and its wall property lies inbetween the more proximal elastic and more peripheral resistive arteries (Struijker-Boudier 2009; Nichols et al. 2011).

In blood vessels where blood transportation is their main function, mean blood volume flow per unit time (q) through a cylindrical vessel has been empirically expressed as a function of its internal vessel radius r , as shown in equation (1) with a real number x :

$$q \propto r^x, \quad (1)$$

which is called the flow-radius relationship (Mayrovitz and Roy 1983; Woldenberg 1983; House and Lipowsky 1987; Horsfield and Woldenberg 1989; Bennett et al. 2000). Hereafter, unless otherwise indicated, the internal radius is simply described as the radius, and all the variables and parameters are expressed in the International System of Units (SI) in equations. When a mother vessel branches into two daughter vessels, representing the blood flow of the mother and of the two daughters as q_m , q_{d_1} , and q_{d_2} , respectively, the preservation of blood flow through these three vessels gives the following

$$q_m = q_{d_1} + q_{d_2}. \quad (2)$$

Moreover, indicating the radii of the mother and her two daughter vessels as r_m , r_{d_1} , and r_{d_2} , respectively, equations (1 and 2) provide us with the relationship between them as

$$r_m^x = r_{d_1}^x + r_{d_2}^x \text{ or } \left(\frac{r_{d_1}}{r_m}\right)^x + \left(\frac{r_{d_2}}{r_m}\right)^x = 1, \quad (3)$$

where x is called the radius exponent (Mandelbrot 1983; Kamiya and Takahashi 2007; Nakamura et al. 2011) or the junction exponent (LaBarbera 1995; Bennett et al. 2000), and corresponds to the fractal dimension of embedding in fractal theory for an asymmetric vascular tree applicable to multiple consecutive arterial generations (Suwa and Takahashi 1971; Mandelbrot 1983; West et al. 1997; Bennett et al. 2000; Gafiychuk and Lubashevsky

2001; Zamir 2001; Kamiya and Takahashi 2007; Nakamura et al. 2011). In normal physiological situations, the mean of x stayed between 2.0 and 3.0, although its range was reported to be from as low as 1.0 to over 4.0 through various methods in a variety of mammalian arteries (Suwa and Takahashi 1971; Sherman 1981; Mayrovitz and Roy 1983; Woldenberg 1983; House and Lipowsky 1987; Horsfield and Woldenberg 1989; Kassab and Fung 1995; LaBarbera 1995; Dawson et al. 1999; Bennett et al. 2000; Zamir 2001; Ghorishi et al. 2007; Nakamura et al. 2011). Hereafter we use suffixes *s* and *p* to indicate systemic and pulmonary, respectively.

Previously reported results of x_s are plotted in Figure 1A against the corresponding r_s , for which we could identify the range. These data mainly reflect $r_s - x_s$ sets listed in LaBarbera's (1995) review article, and include those reported by other studies (Suwa and Takahashi 1971; Sherman 1981; Mayrovitz and Roy 1983; House and Lipowsky 1987; Rossitti and Löfgren 1993; Kassab and Fung 1995; Nakamura et al. 2011). $x_s \approx 2.0-2.3$ was reported by angiographic morphometry in proximal systemic arterial branching structures, such as from the aorta to next-generation large arteries (Zamir and Brown 1982; Zamir et al. 1992; LaBarbera 1995), where little pressure drop takes place. In contrast, $x_s \approx 3$ has consistently been reported in peripheral systemic resistive arteries of $0.004 \leq r_s \leq 0.1$ mm (Nichols et al. 2011) by postmortem cast morphometry in mammals (Sherman 1981; Kassab and Fung 1995) and direct measurement of the $q_s - r_s$ relationship in in vivo rat cremaster arteries (Mayrovitz and Roy 1983; House and Lipowsky 1987). The result of our recent analysis using human hemodynamic data also gave $x_s = 3.1 \pm 0.2$ in peripheral systemic resistive arterial trees, whose radius was assumed to range from 0.01 to 0.1 mm (Nakamura et al. 2011). However, transitional or intermediate values of $x_s \approx 2.7$ have also been observed in several organs of some mammalian systemic arteries (Suwa and Takahashi 1971; LaBarbera 1995; Bennett et al. 2000).

By the same token, we present the pulmonary arterial counterpart reported in humans and dogs in the literature (Suwa and Takahashi 1971; Horsfield and Woldenberg 1989; Dawson et al. 1999; Nakamura et al. 2011) in Figure 1B. Mean x_p was reported to be 2.3 ± 0.1 ($0.0065 \leq r_p \leq 15$ mm) (Horsfield and Woldenberg 1989), or to range from 2.47 ± 0.09 ($r_p < 0.1$ mm) to 2.66 ± 0.07 ($r_p \geq 0.1$ mm) by pulmonary arterial cast morphometry of normal humans (Suwa and Takahashi 1971). Assuming that the peripheral pulmonary arterial radius ranges from 0.01 to 0.1 mm in common with the systemic counterpart, our recent report indicated $x_p = 2.2$ in peripheral pulmonary arteries in normal humans (Nakamura et al. 2011). The relationship

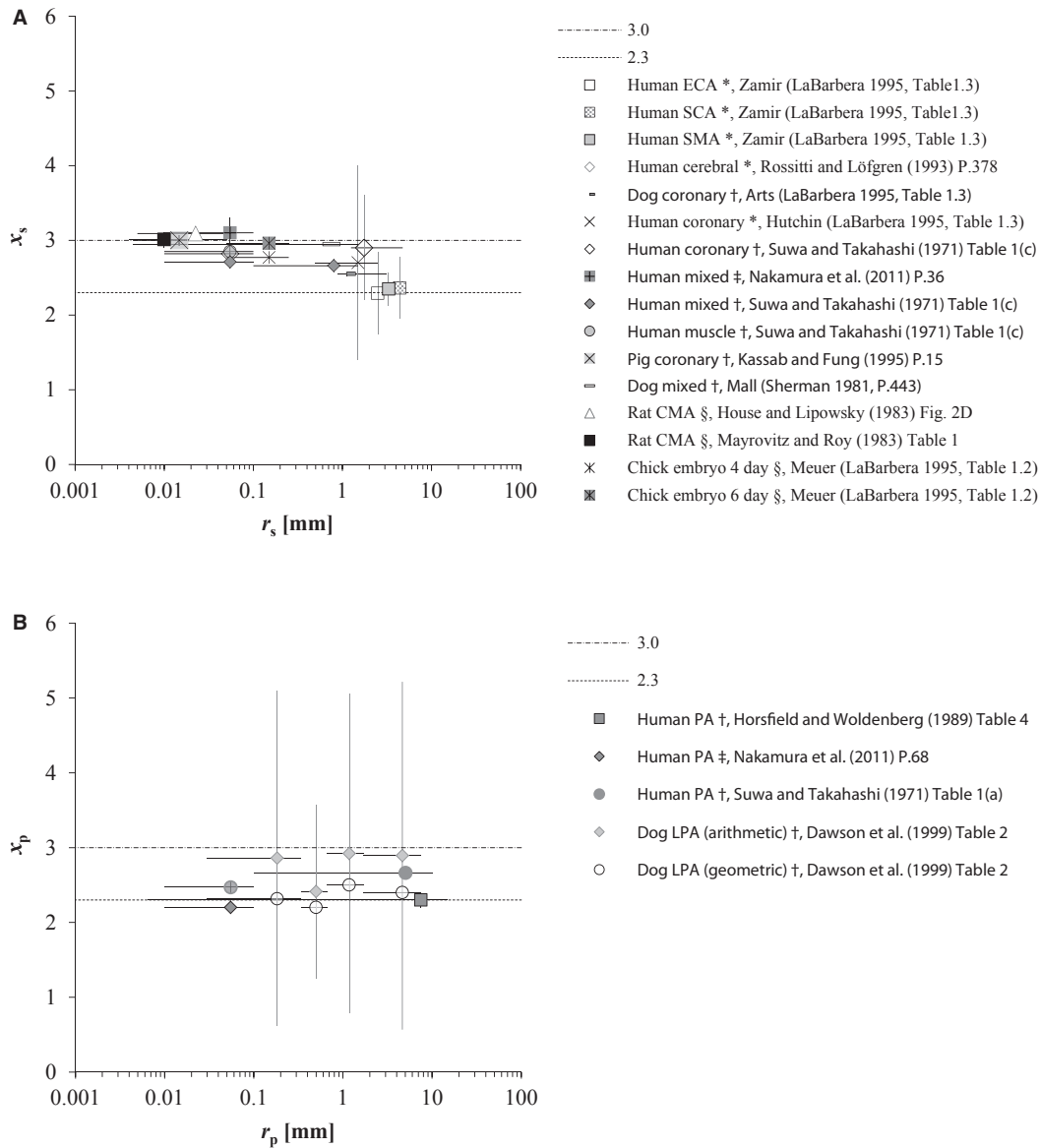


Figure 1. (A) Distribution of reported x_s in a variety of animals by previous studies through various methods, all of which, except for Meuer's data (LaBarbera 1995), are humans (Singhal et al. 1973; Rossitti and Löfgren 1993; LaBarbera 1995; Nakamura et al. 2011) and mammals (Sherman 1981; Mayrovitz and Roy 1983; House and Lipowsky 1987; Kassab and Fung 1995). CMA, ECA, SCA, and SMA indicate the cremaster muscle, external carotid, subclavian, and superior mesenteric arteries, respectively. Radii of ECA, SCA, and SMA were estimated from Olufsen et al.'s (2000) table 1 as 2.5, 4.4, and 3.3 mm, respectively; radius of ECA was tentatively substituted for the mean of the minimal radius at the outlet of bilateral common carotid arteries. House and Lipowsky's (1987) result presented in this figure was derived from the volumetric flow of red blood cells. (B) Distribution of reported x_p in humans (Suwa and Takahashi 1971; Horsfield and Woldenberg 1989; Nakamura et al. 2011) and dogs (Dawson et al. 1999). PA, pulmonary arterial tree; LPA, left PA. r , vessel radius, presented at the mid-point with the range because the mean and median were not reported in the literature; x , radius exponent, defined by in equation (1 or 3) and presented as the mean with one standard deviation. Suffixes s and p indicate systemic and pulmonary. Methodology is indicated by symbols: *angiography; †cast morphometry; ‡model analysis with catheter data; §direct measurement in vivo.

between q_p and r_p in the human pulmonary arterial tree simulated by Singhal et al. (1973) on the basis of their cast morphometry is also presented with a log-log plot in Figure 2, where the slope of this plot clearly indicates that x_p stays constant at 2.32 starting from proximal

large to peripheral small arteries. However, a marked large standard deviation (SD) of the arithmetic mean of x_p around 2.9 was also reported in dog lungs by Dawson et al.'s (1999) cast-morphometric study, as indicated in Figure 1B.

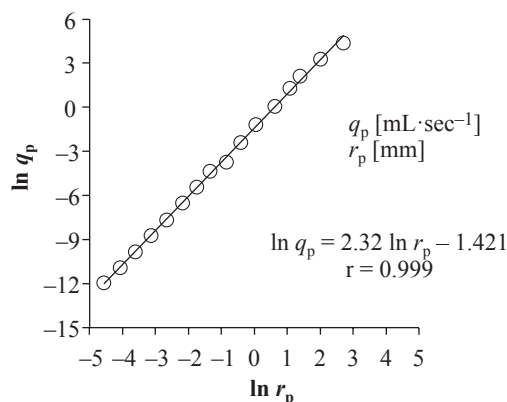


Figure 2. Ln-ln plot of human pulmonary arterial blood flow (q_p) in a vessel against its corresponding vessel radius (r_p). The original data for the plot are derived from combining Singhal et al.'s (1973) tables 4 and 5 under the condition of assumed cardiac output of 4.8 L/min. The slope of this proportionality is equal to radius exponent x . r indicates the correlation coefficient.

To date, the most influential and prevailing theory for $x_s = 3$ found in the peripheral systemic arterial bed (Uylings 1977; Sherman 1981; Zamir and Brown 1982; Rossitti and Löfgren 1993; Kassab and Fung 1995; LaBarbera 1995; Nakamura et al. 2011) is Murray's law, which applied the minimum cost principle to a rigid cylindrical artery with viscous Newtonian steady flow (Murray 1926; Uylings 1977; Sherman 1981; Mayrovitz and Roy 1983; Griffith and Edwards 1990; LaBarbera 1995; Gafiychuk and Lubashevsky 2001; Nakamura et al. 2011). Fractal space-filling embedding (Mandelbrot 1983; Gafiychuk and Lubashevsky 2001) also provides an alternative theoretical basis for $x_s = 3$. However, these two principles are not by themselves effective enough to explain the consistency of the radius exponent of the proximal systemic ($r_s > 1$ [or 2.5] mm) (Zamir and Brown 1982; Zamir et al. 1992; LaBarbera 1995), intermediate systemic elastic-muscular arteries ($0.1 < r_s \leq 1$ [or 2.5] mm) (Suwa and Takahashi 1971; LaBarbera 1995), or the pulmonary arterial beds (Singhal et al. 1973; Horsfield and Woldenberg 1989; Nakamura et al. 2011) on the common basis. Several explanations for x from 2.0 to 2.7 have since been attempted, such as the cross-sectional area-preserving law ($x = 2.0$) (Woldenberg 1983; Zamir et al. 1992; LaBarbera 1995; West et al. 1997; Bennett et al. 2000), minimization of both drag and power loss ($x = 2.0$) (Griffith and Edwards 1990; Bennett et al. 2000), complete turbulence ($x = 7/3 = 2.33$) (Uylings 1977; Bennett et al. 2000), minimization of surface area and power loss ($x = 2.5$) (Griffith and Edwards 1990; Bennett et al. 2000), and minimum volume principle ($2.1 < x < 2.8$) (Woldenberg 1983; Bennett et al. 2000).

Hagen-Poiseuille's equation has long been used universally to express the pressure gradient in arterial models including Murray's theory, irrespective of whether r is derived from big arteries like aorta or from small peripheral arterioles (Murray 1926; Suwa and Takahashi 1971; Uylings 1977; Sherman 1981; Mayrovitz and Roy 1983; Rossitti and Löfgren 1993; Kassab and Fung 1995; LaBarbera 1995; West et al. 1997; Dawson et al. 1999; Gafiychuk and Lubashevsky 2001; Kizilova 2006; Ghorishi et al. 2007; Kamiya and Takahashi 2007; Nakamura et al. 2011). However, it is also well known that Hagen-Poiseuille's equation is unable to accurately estimate vascular resistance in proximal systemic elastic arteries and whole pulmonary arteries because of their large pulsatile fluctuation of radius (Horsfield and Woldenberg 1989; Middleman 1995; Nichols et al. 2011). On the other hand, Bernoulli's equation can and should rather reasonably be applied to blood flow through elastic arteries, such as proximal human systemic or whole pulmonary arteries (Lima et al. 1983a,b; Bermejo et al. 2002; Nichols et al. 2011).

The present article tries to introduce an alternate novel theory for optimal arterial models to explain various values of the radial exponent, which were observed in normal, namely, physiological mammalian arteries from the standpoint of the least energy principle. Prior to the theoretical analysis to follow, referring to Figure 1A and B, we tentatively reviewed the hitherto reported locality, wall property, and radius exponent of systemic and pulmonary arteries, which had been categorized by the radius alone, as shown in Table 1 A and B, because it was considered to provide an overview of the present status of the whole situation surrounding the radius exponent and related morphology.

First, we theoretically used Murray's theory by approaching through the *least energy principle*, where Bernoulli's and Hagen-Poiseuille's equations were, respectively, applied in elastic and rigid arterial models, and we tried to delineate the respective optimal arterial design of these two models in the normal physiological circulation. Second, we also estimated x_s and x_p through mathematical and fractal analysis using previously reported morphometric data of systemic as well as pulmonary arterial trees in the literature. Finally, theoretical results were compared with either reported and/or our own estimated results and discussed in relation to conventional theories.

Methods

Theoretical background

Murray (1926) deliberated on the cost function C for a steady blood flow in a cylindrical artery and came up with the sum of pressure energy loss (ΔU_p) per unit time, as defined by Hagen-Poiseuille's equation on one hand,

Table 1. Categorization of mammalian arteries by locality in terms of radius, arterial wall property, and consequently radius exponent.

Locality	Range of radius (mm)	Wall property	x_s	References
(A) Systemic				
Proximal	$1 < r_s$	Elastic ¹	~2.3	Zamir and Brown (1982); Zamir et al. (1992); LaBarbera (1995)
Intermediate	$0.1 < r_s \leq 1$	Elastic-muscular ²	~2.7	Suwa and Takahashi (1971); LaBarbera (1995)
Peripheral	$0.004 \leq r_s \leq 0.1$	Muscular (rigid) ²	~3.0	Sherman (1981); Mayrovitz and Roy (1983); House and Lipowsky (1987); Kassab and Fung (1995); Nakamura et al. (2011)
Locality	Range of radius (mm)	Wall property	x_p	References
(B) Pulmonary				
Proximal	$0.1 < r_p$	Elastic ¹	~2.3	Singhal et al. (1973); Horsfield and Woldenberg (1989); Dawson et al. (1999)
Peripheral	$0.004 \leq r_p \leq 0.1$	Elastic ¹	~2.3	Singhal et al. (1973); Horsfield and Woldenberg (1989); Dawson et al. (1999); Nakamura et al. (2011)

The range of the radius presented in each classification of systemic and pulmonary arteries comes from Struijker-Boudier's (2009) figure 1 and Suwa and Takahashi's (1971) table 1(a), respectively. r stands for radius; x , radius exponent defined by equation (1 or 3). Suffixes p and s indicate pulmonary and systemic, respectively. Although the lower limit of the vessel radius is common to that of capillaries, our arterial model does not conceptually include the capillary vessel.

^{1,2}indicate vessel types to which we applied our elastic and rigid arterial models, respectively. Data of x came from table 1 (Dawson et al. 1999), table 4 (Horsfield and Woldenberg 1989), figure 2D (House and Lipowsky 1987), P. 15 (Kassab and Fung 1995), table 1.3 (LaBarbera 1995), table 1 (Mayrovitz and Roy 1983), P. 36 (Nakamura et al. 2011), P. 443 (Sherman 1981), tables 4 and 5 (Singhal et al. 1973), and table 3 (Suwa and Takahashi 1971).

and the loss of metabolic energy (ΔU_M) of blood in the vessel per unit time on the other. Indicating pressure loss through the vessel, blood flow rate, internal vessel radius, vessel length, and blood viscosity as ΔP , q , r , l , and μ , respectively, ΔP and ΔU_p were represented as

$$\Delta P = \frac{8\mu l}{\pi r^4} q \quad \text{and} \quad (4)$$

$$\Delta U_p = \Delta P q = \frac{8\mu l}{\pi r^4} q^2, \text{ respectively.} \quad (5)$$

To extend ΔU_M from the original definition by Murray (1926), which was intended only for blood volume in a vessel, to the whole vascular volume, Mayrovitz and Roy (1983) later added the metabolic term of an arterial wall (the second term in the next eq. 6) to that of blood only (the first term) for ΔU_M . Defining the metabolic rate of blood per unit time and volume, that of the vessel wall, and the wall thickness of blood vessels as K_b , K_w , and h (Mayrovitz and Roy 1983), respectively, ΔU_M was represented anew as

$$\Delta U_M = K_b \pi r^2 l + K_w (2\pi r l h). \quad (6)$$

The wall thickness h can be assumed to be constantly proportional to r from large arteries down to micro arterioles and given by $h = wr$, where w is reported by past morphometric studies to be 0.25 in systemic large arteries and 0.2–0.5 in small arteries and arterioles (Uyilings 1977; Mayrovitz and Roy 1983; Nichols et al. 2011). The wall thickness of pulmonary arteries is estimated as one-third of their systemic counterparts (Guyton 1991). Hence,

equation (6) can be rewritten with the aggregated metabolic rate K as

$$\Delta U_M = (K_b + 2wK_w) \pi r^2 l = K \pi r^2 l. \quad (7)$$

Combining equations (5 and 7), Murray's cost function C was defined as (Murray 1926; Mayrovitz and Roy 1983)

$$C = \Delta U_p + \Delta U_M = \frac{8\mu l}{\pi r^4} q^2 + K \pi r^2 l. \quad (8)$$

Applying partial differentiation of C to equation (8) with respect to r , the condition of $\partial C / \partial r = 0$ on the basis of *minimum cost principle* leads to $16\mu q^2 / (K\pi^2) = r^6$, which then results in the next equation (9):

$$q = \frac{\pi}{4} \left(\frac{K}{\mu} \right)^{1/2} r^3. \quad (9)$$

This cubic relationship between q and r is Murray's law itself. However, this persuasive explanation does not necessarily guarantee the minimum cost of the whole arterial tree, where arterial ramifications are essential.

Definition of energy function for an artery

We designed the energy function for a single artery and designated it E , which represents the whole energy needed to drive and transport blood, and maintains both the vessel and the blood. Blood flow was treated as a viscous incompressible Newtonian fluid. Time average or the mean of kinetic, pressure, and metabolic and thermal energies of blood flow are defined as U_K , U_p , and U_M , respectively; the

arterial system transports these three main energies along the stream, as will be detailed later. U_M does not include the metabolic and thermal energy held by the arterial wall in this model, because it is not transported by the arterial stream. Mean losses of kinetic, pressure, and metabolic and thermal energies through the vessel per unit time are represented as ΔU_K , ΔU_P , and ΔU_M , respectively, while ΔU_K and ΔU_P are not significantly dependent upon the shape of branching in this model. We assume that there is no interconversion between dynamic energy (U_K , U_P , ΔU_K , and ΔU_P) and metabolic and thermal energy (U_M and ΔU_M) within the vessel. Energy dissipation due to turbulence of blood flow is not taken into consideration either in this model. The potential energy held by the gravitational center of blood flow and its change through a single artery are not treated separately in this model. While the metabolic energy is partly converted to heat in the whole vascular volume including blood, the movement of heat is assumed to be in equilibrium between the arterial system and the surrounding tissue. The energy conservation through this single artery is expressed as

$$E - (\Delta U_K + \Delta U_P + \Delta U_M) = U_K + U_P + U_M.$$

Thus, we get

$$E = (U_K + \Delta U_K) + (U_P + \Delta U_P) + (U_M + \Delta U_M). \quad (10)$$

Therefore, E is defined as the sum of kinetic energy, pressure energy, metabolic and thermal energy, and loss of each. The rigorous cost function C is definable in equation (10) as

$$C = \Delta U_K + \Delta U_P + \Delta U_M. \quad (11)$$

Minimizing E optimizes the arterial design of this model analysis. However, neither this optimization nor Murray's model incorporates and so guarantees the minimum cost at the arterial branching.

Energy function for an elastic artery

The elastic arterial model is assumed to represent both proximal systemic arteries ($r_s > 1$ mm) (Struijker-Boudier 2009) and the whole pulmonary arterial tree spanning from proximal ($r_p > 0.1$ mm) to peripheral ($0.004 \leq r_p \leq 0.1$ mm) (Singhal et al. 1973; Horsfield 1978; Horsfield and Woldenberg 1989; Huang et al. 1996; Dawson et al. 1999), as indicated also in Table 1A and B. The elastic arterial model is basically assumed cylindrical but might have a modicum of tapering toward the end (Milnor 1982; Dawson et al. 1999; Nichols et al. 2011).

The means of the internal vessel radius and length over time and space in a single elastic artery are indicated as r and l , and the mean blood volume flow per unit time and the mean pressure over time and space

are also represented as q and P , respectively. The pressure drop produced along the length of the vessel is expressed by ΔP .

Indicating the specific gravity of blood as ρ , the mean mass of blood volume flow per unit time is given by ρq . The mean linear velocity v at the gravitational center of blood flow is given as $q/\pi r^2$. Thus, U_K , the kinetic energy of blood flow through the vessel per unit time is expressed in the next equation (12) (Milnor 1982):

$$U_K = \frac{1}{2} \rho q v^2 = \frac{1}{2} \rho q \left(\frac{q}{\pi r^2} \right). \quad (12)$$

In an elastic artery with a modicum of tapering, Bernoulli's effect provides an increase in U_K , which makes ΔU_K negative. U_P and ΔU_P are described as shown below (Milnor 1982):

$$U_P = Pq \quad \text{and} \quad (13)$$

$$\Delta U_P = \Delta Pq \quad (14)$$

Because $1 \mu\text{L}$ O_2 consumption corresponds to 5×10^{-3} cal ($=2.1 \times 10^{-2}$ J) of metabolic energy (Mayrovitz and Roy 1983), U_M is defined as the sum of the metabolic energy converted from the oxygen supply of arterial blood flow and genuine thermal energy in it:

$$U_M = \lambda u_{\text{O}_2} q + c_H q T = (\lambda u_{\text{O}_2} + c_H T) q, \quad (15)$$

where λ , u_{O_2} , c_H and T indicate the proportional coefficient to convert oxygen volume in blood to equivalent metabolic energy ($\lambda = 2.1 \times 10^4$ J L^{-1}), the arterial oxygen volume per unit blood volume, the specific heat capacity of blood per unit volume, and the mean absolute temperature of blood as an average over time and space, respectively. u_{O_2} is regarded as constant throughout the arterial tree in this model for simplification.

Furthermore, ΔU_M in this article is defined again in equation (7) as in Murray's or Mayrovitz and Roy's equations; however, the $l - r$ relationship of an arterial tree in a number of human organs has already been reported by Suwa and Takahashi (1971), who indicated that l was a function of r using real numbers α and Ω in both systemic and pulmonary arteries as

$$l = \Omega r^\alpha \quad (16)$$

This empirical expression has been applied widely in arterial fractal models (Suwa and Takahashi 1971; West et al. 1997; Dawson et al. 1999; Olufsen et al. 2000; Gafiychuk and Lubashevsky 2001; Kizilova 2006; Kamiya and Takahashi 2007). The morphologically estimated value of the exponent α centers around 1.0, ranging from 0.76 to 1.21, in various human systemic (Suwa and Takahashi 1971; Kamiya and Takahashi 2007) as well as mammalian pulmonary arteries (Suwa and Takahashi 1971; Dawson et al. 1999), as listed in Table 2. Simply

assumed to be 1.0, it has generally been used and discussed in model studies (Suwa and Takahashi 1971; West et al. 1997; Dawson et al. 1999; Olufsen et al. 2000; Gafiychuk and Lubashevsky 2001; Kizilova 2006; Kamiya and Takahashi 2007). Therefore, when we need to deal with α in this model analysis, α is set tentatively to 1.0 for the sake of simplicity and brevity. As a result, equation (7) was rewritten with equation (16) as

$$\Delta U_M = K\pi\Omega r^{2+\alpha}. \tag{17}$$

Substitution of equations (12–15 and 17) into equation (10) gives

$$E = \frac{1}{2}\rho q \left(\frac{q}{\pi r^2}\right)^2 + \Delta U_K + (P + \Delta P)q + (\lambda u_{O_2} + c_H T)q + K\pi\Omega r^{2+\alpha}. \tag{18}$$

Because Bernoulli's effect always guarantees reciprocal conversion between ΔU_K and ΔU_P as $\Delta U_K + \Delta U_P \approx 0$ throughout an elastic artery (Lima et al. 1983a,b; Bermejo et al. 2002; Nichols et al. 2011), $\Delta U_K + \Delta Pq \approx 0$ also holds true in equation (18).

In conclusion, equation (18) is rewritten with Bernoulli's effect as

$$E = \frac{1}{2}\rho q \left(\frac{q}{\pi r^2}\right)^2 + Pq + (\lambda u_{O_2} + c_H T)q + K\pi\Omega r^{2+\alpha}. \tag{19}$$

We partially differentiated E with respect to r , and applied $\partial E/\partial r = 0$ to equation (19).

Energy function for a rigid artery

The rigid arterial model is applied to intermediate ($0.1 < r_s \leq 1$ mm) (Struijker-Boudier 2009; Nichols et al. 2011) and peripheral systemic arteries ($0.004 \leq r_s \leq 0.1$ mm) (Mayrovitz and Roy 1983; House and Lipowsky 1987; Nichols et al. 2011), both of which we regard as cylindrical (Murray 1926; Suwa and Takahashi 1971; Uylings 1977; Sherman 1981; Mayrovitz and Roy 1983; Kassab and Fung 1995; LaBarbera 1995; West et al. 1997; Olufsen et al. 2000; Gafiychuk and Lubashevsky 2001; Kizilova 2006; Kamiya and Takahashi 2007; Nakamura et al. 2011; Nichols et al. 2011), as indicated in Table 1A. The energy function E in equation (10) was also applied to the analysis of the optimal design of a rigid artery. U_K , U_P , U_M , and ΔU_M are similarly expressed as counterparts in equations (12, 13, 15, and 17), respectively. As ΔU_P in a rigid artery is due to the friction between viscous blood flow and the arterial inner surface (Nichols et al. 2011), Hagen-Poiseuille's equation was applied as presented in equation (5). Because there is no change in mean linear velocity through a rigid artery due to Hagen-Poiseuille's law, ΔU_K is equal to 0 in equation (10). By substituting

Table 2. Reported data of α and Ω in systemic and pulmonary arteries by previous studies of fractal analysis with cast-morphometric measurements in the literature.

	Reference	Range of radius (mm)	α	Ω
Systemic				
Human renal	Suwa and Takahashi (1971)	≥ 0.01	0.85	17.6
Mesenteric	Suwa and Takahashi (1971)	≥ 0.01	1.04	13.0
Femoral	Suwa and Takahashi (1971)	≥ 0.01	1.01	13.2
Pancreas	Suwa and Takahashi (1971)	≥ 0.01	0.90	16.1
Cerebral cortex	Suwa and Takahashi (1971)	≥ 0.01	1.15	7.4
Basal ganglion	Suwa and Takahashi (1971)	≥ 0.01	1.21	4.6
Coronary	Suwa and Takahashi (1971)	≥ 0.01	1.05	7.9
Pulmonary				
Human ¹	Dawson et al. (1999)	0.0065–0.425	0.85	6.43
Human ²	Dawson et al. (1999)	0.01–7.4	0.89	9.51
Human	Suwa and Takahashi (1971)	≥ 0.01	1.16	2.8
Dog lt.	Dawson et al. (1999) ⁵	0.030–7.574	1.139–1.15	3.987–5.0
Dog	Dawson et al. (1999)		1.00	
Dog ³	Dawson et al. (1999)	0.014–5.56	0.84	9.72
Cat	Dawson et al. (1999)		1.03	15.5
Rat ⁴	Dawson et al. (1999)	0.00665–0.8	1.03	5.3

α and Ω represent exponent and proportional coefficient of the relationship between vessel length and radius, respectively, defined by equation (16); lt, left. Research articles which Dawson et al. (1999) used for their estimation are partly common to our references (Horsfield 1978; Gan and Yen 1994; Jiang et al. 1994; Huang et al. 1996).

^{1,2,3,4} corresponded to the above-mentioned Horsfield (1978); Huang et al. (1996); Gan and Yen (1994); Jiang et al. (1994), respectively. Sources of data were table 3 (Suwa and Takahashi 1971) and table 1 (Dawson et al. 1999), while ⁵ means figure 4 (Dawson et al. 1999).

equation (16) into equation (5) as ΔU_p , E of a rigid cylindrical artery is finalized as

$$E = \frac{1}{2} \rho q \left(\frac{q}{\pi r^2} \right)^2 + Pq + \frac{8\mu\Omega r^\alpha}{\pi r^4} q^2 + (\lambda u_{O_2} + c_H T)q + K\pi\Omega r^{2+\alpha}, \quad (20)$$

which involves the addition of Hagen-Poiseuille's term in equations (5–19) as a consequence. Similarly, the optimal relationship between q and r was sought by $\partial E/\partial r = 0$.

Resources of subjected data

For comparison, we also analyzed mammalian arterial cast-morphometric data sets reported in the literature, which contain r , l , and the number of vessels in an arterial tree in each generation. The rule of vessel generation is ranked and numbered at each ramification from the most proximal to the most peripheral arteries. However, if the literature in question happened to follow the rule of “order,” which adopted an inverse numbering system starting from the most peripheral arteries, we regarded the largest order as the first generation, revising orders into generations. One data set of canine mixed systemic arterial trees was available from Milnor's (1982) morphometric study. We also used Mall's data of canine superior mesenteric arterial tree modified by Sherman (1981), who adopted the rule of “rank,” which numbered the first-generation vessel as 0, although Mall's data set lacks data about l . We could also acquire three human pulmonary arterial data sets from Horsfield's (1978), Huang et al.'s (1996), and Singhal et al.'s (1973) postmortem cast-morphometric studies. Data in Huang et al. (1996) and Singhal et al. (1973) were from a 44-year-old man and a 32-year-old woman, respectively. Because table 6 in Horsfield (1978) was a revised data set of the human pulmonary arterial tree from table 4 of Singhal et al. (1973) by amending vessel numbers in small arteries ($0.013 \leq r_p \leq 0.850$ mm) (Horsfield 1978), our analysis did not include the data from order 11 to 17 ($1.33 \leq r_p \leq 30$ mm) in Horsfield (1978), which were common to those in Singhal et al. (1973). In addition, four mammalian data sets of the pulmonary arterial tree were subjected to our analysis; Gan and Yen's (1994) and Milnor's (1982) dog, Zhuang et al.'s (1983) cat, and Jiang et al.'s (1994) rat cast-morphometric data. Data from two other studies (Olufsen et al. 2000; Nakamura et al. 2011) were also used.

Data analysis of x , α , and Ω

Radial exponent x was estimated in each succeeding generation through the arterial tree of morphometric data

sets. Letting n be a natural number, we assume that the n th generation mother arteries with mean internal radius r_n and mean vessel length l_n branch into the $(n+1)$ th generation daughter arteries with mean internal radius r_{n+1} and mean vessel length l_{n+1} , while the vessel numbers of the n th and the $(n+1)$ th generation arteries are represented as N_n and N_{n+1} , respectively. Defining the ratios of the radius, length, and vessel number of the $(n+1)$ th generation to the n th as β_n ($0 < \beta_n < 1$), γ_n ($0 < \gamma_n < 1$), and η_n (>1), we indicate the means of β_n , γ_n , and η_n through consecutive generations as β , γ , and η , respectively. Branching rules (West et al. 1997; Ghorishi et al. 2007; Nakamura et al. 2011) are given as

$$\beta_n = \frac{r_{n+1}}{r_n}, \gamma_n = \frac{l_{n+1}}{l_n}, \text{ and } \eta_n = \frac{N_{n+1}}{N_n}. \quad (21)$$

Using x_n as the radial exponent between n th and $(n+1)$ th generations, the preservation of blood flow through ramifications ensures the following

$$N_n r_n^{x_n} = N_{n+1} r_{n+1}^{x_n}. \quad (22)$$

Equation (22) gives x_n as

$$x_n = \frac{\ln(N_n/N_{n+1})}{\ln(r_{n+1}/r_n)} = -\frac{\ln \eta_n}{\ln \beta_n}. \quad (23)$$

Means and SD of x_n were computed in respective arterial categories by the radius, as given in Table 1A and B, and are presented as estimated x .

α was estimated from equation (16) as the slope of linear regression analysis between $\ln r$ versus $\ln l$ (Suwa and Takahashi 1971; Dawson et al. 1999), where the vertical intercept corresponded to $\ln \Omega$ throughout each arterial category as listed in Table 1A and B. By combining equations (16 and 21) as

$$\alpha = \frac{\ln \gamma}{\ln \beta}, \quad (24)$$

we alternatively sought α from the results of β and γ , which were reported in our previous study (Nakamura et al. 2011). We also computed Ω from Olufsen et al.'s (2000) data under $\alpha = 1.0$.

Statistical analysis

The decision of a statistically significant outlier was made by Dixon's Q test, which defines the estimator Q as a statistical value obtained by dividing the gap by the full range of sample data, where gap means the absolute difference between the outlier in question and the closest value to it (Böhler 2008). When Q exceeded the critical value of confidential limit under $P < 0.05$, the outlier was excluded from further statistical analysis (Böhler 2008).

Results

The elastic arterial system

Because $\partial E/\partial r = 0$ in equation (19) results in $2\rho q^3 = (2 + \alpha)K\pi^3\Omega r^{6+\alpha}$, it follows

$$q = \pi \left\{ \left(\frac{2 + \alpha}{2} \right) \frac{K\Omega}{\rho} \right\}^{1/3} r^{2+\alpha/3}. \quad (25)$$

Hence, x was directly derived from equations (1 and 25) as follows:

$$x = 2 + \frac{\alpha}{3}. \quad (26)$$

When α is assumed equal to 1.0, x is deduced as 2.33. Equation (3) is also written with equation (26) as

$$\left(\frac{r_{d1}}{r_m} \right)^x + \left(\frac{r_{d2}}{r_m} \right)^x = \left(\frac{r_{d1}}{r_m} \right)^{2+\alpha/3} + \left(\frac{r_{d2}}{r_m} \right)^{2+\alpha/3} = 1. \quad (27)$$

Using α , β , γ , and η on the basis of equations (21, 22, and 24), the preservation of blood flow extends equation (27) into an asymmetric fractal expression (Mandelbrot 1983; Kamiya and Takahashi 2007; Nakamura et al. 2011):

$$\eta\beta^x = \eta\beta^{2+\alpha/3} = \eta\beta^2\gamma^{1/3} = 1. \quad (28)$$

Equation (28) shows that $x = 2 + \alpha/3$ of equation (26) retains its validity both structurally and functionally even in the case of more complex asymmetric ramifications.

The rigid arterial system

$\partial E/\partial r = 0$ as applied to equation (20) gave

$$\left(\frac{2}{2 + \alpha} \right) \frac{\rho}{K\pi^3\Omega} q^3 + \left(\frac{4 - \alpha}{2 + \alpha} \right) \frac{8\mu}{K\pi^2} q^2 = r^6. \quad (29)$$

Letting q/r be f for convenience, x is given below in equation (30) by taking α as 1.0 only at the exponent in equation (29) (Appendix A1):

$$x \cong 2 + \frac{(\rho f/\pi\mu) + 8(4 - \alpha)\Omega}{3(\rho f/\pi\mu) + 8(4 - \alpha)\Omega}. \quad (30)$$

Using $v = q/\pi r^2$, $f = q/r$, and $D = 2r$, where D stands for the internal vessel diameter, Reynolds number (Re) is defined and rewritten as shown in next equation (31) (Horsfield and Woldenberg 1989; Nichols et al. 2011):

$$Re = \frac{vD\rho}{\mu} = \frac{2\rho q}{\pi\mu r} = \frac{2\rho f}{\pi\mu}. \quad (31)$$

Eliminating f in equation (30) using equation (31), we can express x with Re and Ω as

$$x \cong 2 + \frac{\zeta}{3}, \text{ where, } \zeta = \frac{Re + 16(4 - \alpha)\Omega}{Re + 16(4 - \alpha)\Omega/3}. \quad (32)$$

Equation (32) indicates that mean x asymptotically approaches its upper limiting value of 3.00 at $Re < 10$ and to its lower limiting value $7/3 = 2.33$ at $Re > 10^4$. Using α , β , γ , and η again, the blood flow preservation also guarantees equation (32) in an asymmetric arterial fractal by the same token as previously applied to the elastic arterial system:

$$\eta\beta^x = \eta\beta^{2+\zeta/3} = \eta\beta^2\gamma^{\zeta/3\alpha} = 1. \quad (33)$$

Estimation of x , α , and Ω from the literature

Distribution diagrams of the estimated x_s and x_p against r_s and r_p , respectively, are presented in Figure 3A and B. Mean and SD of the estimated x_s and x_p in each categorized group by radius, as indicated in Table 1A and B are shown in Table 3A and B, respectively. Table 3A does not include the result of $x_s = 5.56$ at $r_s = 0.026$ mm from Sherman's rank 4 arteries in Mall's data (Sherman 1981) (our fifth generation equivalents) because the Q value resulted in 0.831 ($= (5.56 - 3.36)/(5.56 - 2.91)$) over the critical value of 0.829 ($P < 0.05$) (Böhrer 2008) among four estimates in the peripheral arterial area, as indicated in Figure 3A. Estimated α and Ω of systemic and pulmonary arterial trees are presented in Table 4A and B, respectively. Available systemic arterial data for this analysis were too scarce to separately estimate the parameters from these three groups, as classified in Table 1A.

Comparison of theoretically derived x with morphometrically determined x_s and x_p

$x = 2.33$ from equation (26) was compared with estimated and reported data of proximal systemic arterial x_s , and proximal and peripheral pulmonary arterial x_p , in Figure 4A ($r_s > 1$ mm) and Figure 4B, respectively. Equation (32) was plotted in Figure 4A together with reported and our estimated mean x_s after adjusting the range of r_s to the corresponding Re as follows. First in the proximal systemic artery, average Re values at the aortic bifurcation and in the common iliac arteries were reported to range between 400 and 1100 (mean, 730), and between 390 and 620, respectively (Nichols et al. 2011). Second, when ρ of 1.06 mg/cm³ and μ of 0.04 Poise ($\text{g cm}^{-3} \text{sec}^{-1}$) are substituted for equation (31) (Horsfield and Woldenberg 1989; Kamiya and Takahashi 2007; Nichols et al. 2011), Re can be represented in the following equation:

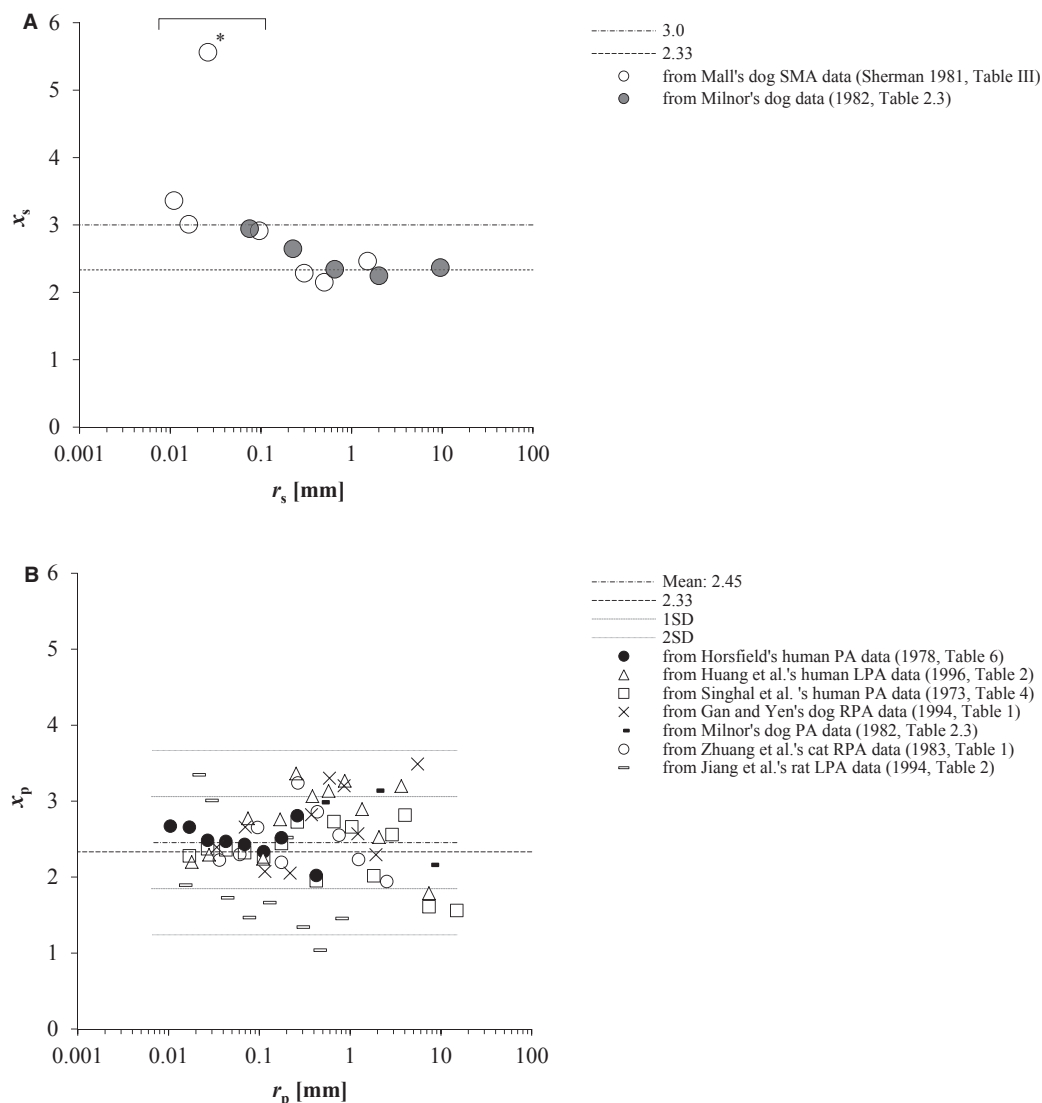


Figure 3. (A) Plot of estimated x_s vs. r_s at each arterial generation of systemic arteries of two dogs in the literature (Sherman 1981; Milnor 1982). *indicates the result regarded as an outlier by Q test ($P < 0.05$) (Böhner 2008) among the estimates from Mall's data of dog superior mesenteric arteries (SMA) (Sherman 1981) at peripheral systemic arterial area ($0.004 \leq r_s \leq 0.1$ mm). (B) Counterparts of pulmonary arteries from three human (Singhal et al. 1973; Horsfield 1978; Huang et al. 1996) and four mammalian data (Milnor 1982; Zhuang et al. 1983; Gan and Yen 1994; Jiang et al. 1994) in the literature. Mean of all estimated x_p was indicated together with single and double standard deviations by broken and dotted lines, respectively. PA, pulmonary arterial tree; LPA, left PA; RPA, right PA. r , vessel radius; x , radius exponent, defined by in equation (1 or 3); s, systemic; p, pulmonary.

$$Re = \frac{q}{\pi r^2} \frac{2r\rho}{\mu} = \frac{2 \times 1.06 q}{\pi \times 0.04 r} = 16.88 \frac{q}{r}, \quad (34)$$

where q and r are given in cgs unit (Nichols et al. 2011). Mayrovitz and Roy (1983) reported the regression equation as $q_s = 200 \times D_s^{2.89}$ in cgs unit, where q_s and D_s represented mean blood flow in an artery (cm^3/sec) and its vessel diameter (cm) ranging between 0.0006 and 0.0108 cm, respectively, in an in vivo direct micro-

scopic measurement of cremaster muscle arteries of rats. Applying the result reported by Mayrovitz and Roy to equation (34) by expanding the range of r_s to 0.1 mm, we were able to estimate Re as 4.2 ($=16.88 \times 200 \times (0.02)^{2.89}/0.01$) at $r_s = 0.1$ mm. Therefore, average Re is considered to reside within the range of 4 and 400 in the region of intermediate systemic arteries. Several coupled conditions of physiological Ω and Re_s , under which equation (32) gives x_s of 2.7, are presented in Table 5.

Table 3. Estimated data of x in systemic (A) and pulmonary arteries (B) from reported data sets by previous studies.

References		Range of r_s (mm)	x_s
(A) Systemic arteries			
Proximal		$1 < r_s$	
Dog	Milnor (1982)	2–9.5	2.32 ± 0.06
Dog SMA	Sherman (1981)	1.5	2.46
Intermediate		$0.1 < r_s \leq 1$	
Dog	Milnor (1982)	0.225–0.65	2.49
Dog SMA	Sherman (1981)	0.3–0.5	2.22 ± 0.09
Peripheral		$0.004 \leq r_s \leq 0.1$	
Dog	Milnor (1982)	0.075	2.95
Dog SMA	Sherman (1981)	0.011–0.016	3.10 ± 0.24^1
References		Range of r_p (mm)	x_p
(B) Pulmonary arteries			
Proximal		$0.1 < r_p$	
Human	Horsfield (1978)	0.112–0.425	2.42 ± 0.33
Human lt.	Huang et al. (1996)	0.11–7.4	2.82 ± 0.50
Human	Singhal et al. (1973)	0.112–15	2.30 ± 0.46
Dog rt.	Gan and Yen (1994)	0.14–5.56	2.72 ± 0.57
Dog	Milnor (1982)	0.5–8.0	2.76 ± 0.52
Cat rt.	Zhuang et al. (1983)	0.176–2.54	2.50 ± 0.51
Rat lt.	Jiang et al. (1994)	0.13–0.8	1.60 ± 0.56
Peripheral		$0.004 \leq r_p \leq 0.1$	
Human	Horsfield (1978)	0.0065–0.069	2.54 ± 0.11
Human lt.	Huang et al. (1996)	0.01–0.075	2.42 ± 0.31
Human	Singhal et al. (1973)	0.011–0.069	2.33 ± 0.04
Dog rt.	Gan and Yen (1994)	0.014–0.070	2.52 ± 0.19
Cat rt.	Zhuang et al. (1983)	0.012–0.096	2.39 ± 0.23
Rat lt.	Jiang et al. (1994)	0.00665–0.078	2.29 ± 0.83

r stands for vessel radius; x , radius exponent, defined by equation (1 or 3); s , systemic; p , pulmonary. SMA indicates superior mesenteric artery; lt, left; rt., right. ¹excluded the rank 4 arterial data (Sherman 1981) as an outlier. Vessels are categorized in terms of the radius by the classification presented in Table 1A and 1B. Data of the whole pulmonary arterial tree are indicated with no notation of laterality. The present analysis used table 1 (Gan and Yen 1994), table 6 (Horsfield 1978), table 2 (Huang et al. 1996), table 2 (Jiang et al. 1994), table 2.3 (Milnor 1982), table III (Sherman 1981), table 4 (Singhal et al. 1973), and table 1 (Zhuang et al. 1983). Data are presented as the mean with one standard deviation.

Thirdly, Re at $D_s = 0.1$ mm ($r_s = 0.05$ mm) in an intra-organ arterial bed was reported to be 0.1 by theoretical simulation by Kizilova (2006). Thus, average Re in arteries of $r_s \leq 0.1$ mm is supposed to range approximately between 0.1 and 4. Values of Re in the range from 0.1 to 4 yielded $x_s = 3.00$ with equation (30) (Fig. 4A), where Ω_s spanned from 60 to 70 in peripheral systemic arteries (Table 4A).

Discussion

Application of the least energy principle to E for both elastic and rigid arterial models yielded the optimal x for each model. Irrespective of whether it is elastic or rigid, these results in a single arterial model could successfully be extended even to an asymmetric fractal arterial tree system from the viewpoint of blood flow preservation at branchings. Neither blood temperature in equation (15) nor metabolic rates of K_b and/or K_w in equation (6) influenced optimal arterial fractal structures in this model analysis. We can regard T as independent of the radius in general. K_b and/or K_w , whose estimated values based on experimental data were reported to be 4.34×10^3 and 29.9×10^3 erg cm⁻³ sec⁻¹, respectively, by the detailed study of Mayrovitz and Roy (1983), were also independent of the radius in previous model studies (Murray 1926; Uylings 1977; Sherman 1981; Mayrovitz and Roy 1983; Griffith and Edwards 1990; Gafiychuk and Lubashevsky 2001). However, if the local environment happens to change u_{O_2} and T as well as K_b and K_w , the optimal x cannot in all likelihood escape their influence. The Fåhræus-Lindqvist effect (Dawson et al. 1999; Kamiya and Takahashi 2007; Nakamura et al. 2011; Nichols et al. 2011), which is well known as a non-Newtonian effect, will yield a smaller x than the predicted value of 3.0 by equation (32) in the peripheral systemic arteries because this effect raises Re by significantly decreasing μ under the condition of $0.004 \leq r_s \leq 0.2$ mm (Kamiya and Takahashi 2007; Nichols et al. 2011).

The arrangement of x_s obtained from two canine data sets (Sherman 1981; Milnor 1982) in Figure 3A proved similar to the inverse-sigmoid curve in Figure 4A, suggesting a multifractal vascular system (Zamir 2001; Grasman et al. 2003). Equation (32) under several physiological conditions of Ω and Re (Table 5), which yields x around 2.7, partly explained quantitatively this tendency of reported or estimated x_s distribution at intermediate systemic arteries ($0.1 < r_s \leq 1$ mm) (Fig. 4A). Alternatively, we can get $Re = 13.1 \Omega$ by substituting both $x = 2.7$ and $\alpha = 1.0$ into equation (32). Estimated mean x_s for proximal ($r_s > 1$ mm) and peripheral systemic arteries ($0.004 \leq r_s \leq 0.1$ mm) from Milnor (1982) and Sherman (1981) agreed with the pertinent morphometric and hemodynamic data in the literature (Sherman 1981; Zamir and Brown 1982; Mayrovitz and Roy 1983; House and Lipowsky 1987; Kassab and Fung 1995; LaBarbera 1995; Nakamura et al. 2011), as indicated in Table 3A. While x_s for intermediate systemic arteries ($0.1 < r_s \leq 1$ mm) from Milnor's (1982) data was estimated to be a little smaller than the expected value of 2.7, that from the modified Mall's data (Sherman 1981) estimated as 2.2 turned out to be closer to that of more proximal

Table 4. Estimated data of α and Ω in systemic (A) and pulmonary arteries (B) by fractal analysis with published data in the literature.

References		Range of radius (mm)			α_s	Ω_s	r			
<i>(A) Systemic arteries</i>										
Human Ao	Olufsen et al. (2000)	7.2–12.0				3.3 ± 2.5^1				
CCA		2.8–2.9				63.1 ± 5.0^1				
Maj. brs.		1.9–7.0				17.9 ± 7.6^1				
Human mixed	Nakamura et al. (2011)	0.01–0.1			0.78 ²					
Dog mixed	Milnor (1982)	0.025–9.5			1.11	70.66	0.99			
References		Whole tree			Proximal ($0.1 \text{ mm} < r_p$)			Peripheral ($0.004 \leq r_p \leq 0.1 \text{ mm}$)		
		α_p	Ω_p	r	α_p	Ω_p	r	α_p	Ω_p	r
<i>(B) Pulmonary arteries</i>										
Human	Horsfield (1978)	0.85	9.21	0.99	0.97	11.53	0.97	0.83	8.61	0.99
Human lt.	Huang et al. (1996)	0.89	9.38	0.98	0.86	9.69	0.96	0.55	2.61	0.98
Human	Nakamura et al. (2011)							0.71 ²		
Human	Singhal et al. (1973)	0.80	8.09	0.99	0.76	8.31	0.97	0.83	8.61	0.99
Dog rt.	Gan and Yen (1994)	0.83	13.13	0.99	0.77	13.30	0.97	0.92	16.51	0.99
Dog	Milnor (1982)	0.68	8.46	0.91						
Cat rt.	Zhuang et al. (1983)	1.03	14.11	0.99	0.78	13.01	0.95	1.21	24.77	0.99
Rat lt.	Jiang et al. (1994)	0.72	2.17	0.98	0.83	2.29	0.97	0.93	5.20	0.98

α and Ω represent exponent and proportional coefficients of the relationship between vessel length (l) and radius (r), respectively, defined by equation (16); r , correlation coefficient; s , systemic; p , pulmonary; $lt.$, left; $rt.$, right. Pulmonary arteries were categorized by radius; each range of the radius in subjected data is not indicated but is common to Table 3B. The data included in the present analysis came from table 1 (Gan and Yen 1994), table 6 (Horsfield 1978), table 2 (Huang et al. 1996), table 2 (Jiang et al. 1994), table 2.3 (Milnor 1982), P. 68 (Nakamura et al. 2011), table 1 (Olufsen et al. 2000), table 4 (Singhal et al. 1973), and table 1 (Zhuang et al. 1983). All methods but two (Olufsen et al. 2000; Nakamura et al. 2011) were cast-morphometry; that of Nakamura et al. (2011), the combination of fractal-model analysis and catheterization; that of Olufsen et al. (2000), measurement on magnetic resonance images or estimation. Ao stands for aorta, which includes ascending aorta, aortic arch, and abdominal aorta (Olufsen et al. 2000); CCA, common carotid arteries; Maj. brs., major branches, which include superior and inferior mesenteric, renal, internal and external iliac, and superficial and deep femoral arteries (Olufsen et al. 2000). Data of the whole pulmonary arterial tree are indicated with no notation of laterality.

¹indicates estimates under $\alpha = 1.0$.

²was calculated by equation (24). Data are presented as the mean with one standard deviation.

elastic arteries (Table 3A). Because x_s , which we think is largely affected by wall properties, would also vary among regions, animal species and, most of all, among individuals even with the same radius, the property of intermediate elastic-muscular arteries might be identified not by the scale of r_s alone, but rather by x_s itself, as presented in Table 6. While x_s from the rank 4 (fifth generation) arteries of modified Mall's data was regarded as an outlier by the Q test in this analysis, Sherman originally mentioned that Mall's data of rank 3 ($r_s = 0.096 \text{ mm}$) and four ($r_s = 0.026 \text{ mm}$) arteries were questionable due to a systematic distortion in the size of some of the small arteries, since the dogs in Mall's study were killed by bleeding, with the result of probably pronounced vasoconstriction (Sherman 1981).

Mean estimated x_p from the data of normal mammalian pulmonary arterial morphometry in the literature (Singhal et al. 1973; Horsfield 1978; Zhuang et al. 1983; Gan and Yen 1994; Jiang et al. 1994; Huang et al. 1996;

Nakamura et al. 2011) focused around 2.3–2.5 in both proximal ($r_p > 0.1 \text{ mm}$) and peripheral pulmonary arteries ($0.01 \leq r_p \leq 0.1 \text{ mm}$) as displayed in Table 3B and Figure 4B. However, it will not be justified so easily to regard x_p as monofractal throughout the whole pulmonary arterial tree because the distribution of individually estimated x_p exhibited an actually large range at proximal pulmonary arteries, as presented in Figure 3B. Marked fluctuation of x_p at these proximal pulmonary arteries can be attributed to such factors as their varied elliptical cross section (Milnor 1982; Nichols et al. 2011), significant tapering structure of the main pulmonary artery toward its first branches (Milnor 1982; Dawson et al. 1999), and the inherent constraints imposed, more or less, on these vessels by the shape of the thoracic cage, lungs, and heart (Singhal et al. 1973). However, estimated peripheral x_p of three humans (Singhal et al. 1973; Horsfield 1978; Huang et al. 1996) converged at 2.41 ± 0.18 in the range of r_p below 0.1 mm, as shown in Figure 3B,

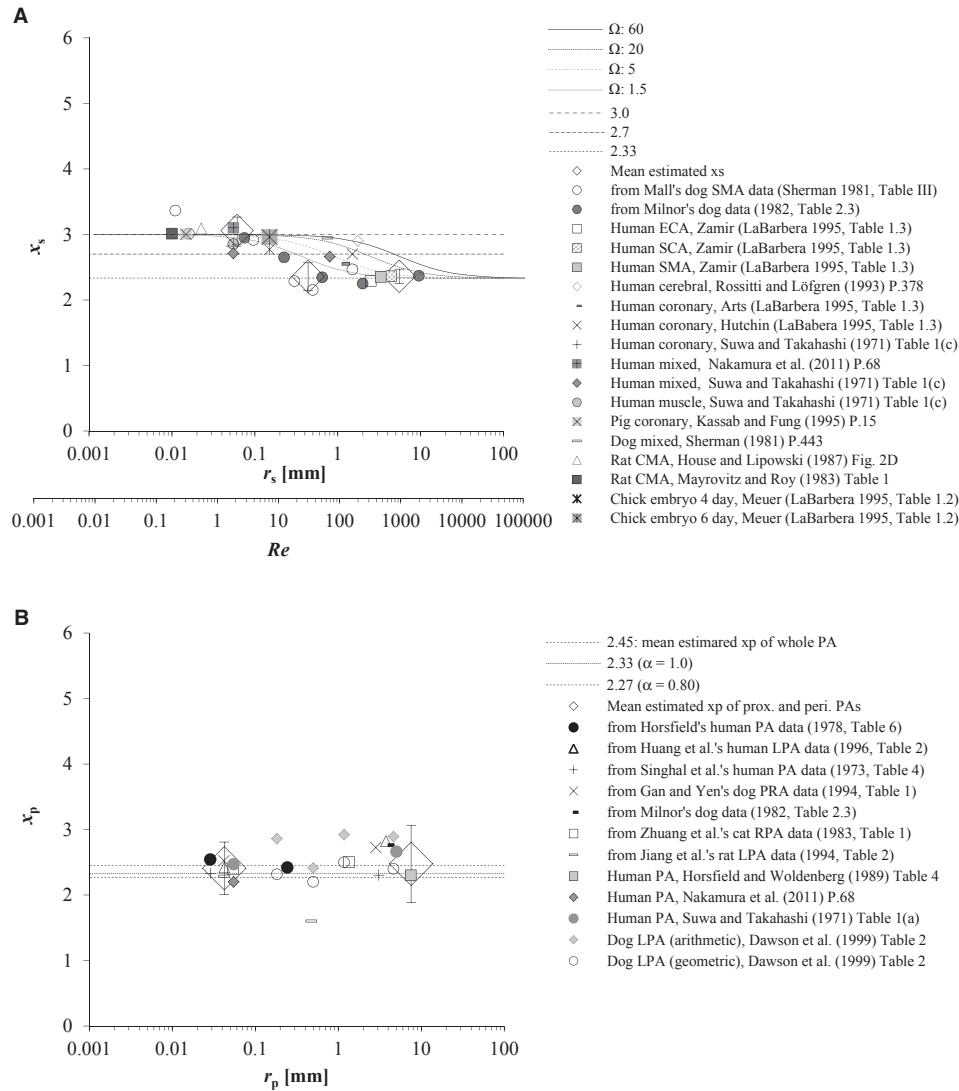


Figure 4. (A) Comparison between theoretical x from our rigid arterial model and morphometric x_s . The model-derived optimal relationship between the radius exponent x vs. Reynolds number (Re) in a rigid cylindrical artery was also plotted as curves based upon equation (32), which shift to the right with the increment of Ω . Ω represents the proportional coefficient of the vessel length-radius relationship in equation (16). Both reported mean x_s in the literature (Suwa and Takahashi 1971; Sherman 1981; Mayrovitz and Roy 1983; House and Lipowsky 1987; Rossitti and Löfgren 1993; Kassab and Fung 1995; LaBarbera 1995; Nakamura et al. 2011) and those estimated from two dog data in previous studies (Sherman 1981; Milnor 1982) were plotted together against corresponding r_s . Mean and one standard deviation (SD) of the estimates were plotted with large rhombuses and outliers, respectively, at proximal (x_s , 2.36 ± 0.11 ; r_s , 5.5 mm, range 1.5–9.5 mm), intermediate (x_s , 2.36 ± 0.21 ; r_s , 0.44 mm, range 0.23–0.65 mm), and peripheral arterial regions (x_s , 3.06 ± 0.21 ; r_s , 0.06 mm, range 0.01–0.10 mm), where Mall's rank 4 (corresponding to our 5th generation) arterial data (Sherman 1981) were excluded as an outlier. CMA, ECA, SCA, and SMA indicate the cremaster muscle, external carotid, subclavian, and superior mesenteric arteries, respectively. (B) Comparison between the elastic arterial model-derived x and morphometric x_p . Means of both reported x_p in the literature (Suwa and Takahashi 1971; Horsfield and Woldenberg 1989; Dawson et al. 1999; Nakamura et al. 2011) and those estimated from published data sets (Singhal et al. 1973; Horsfield 1978; Milnor 1982; Zhuang et al. 1983; Gan and Yen 1994; Jiang et al. 1994; Huang et al. 1996) were similarly plotted together against r_p . Large rhombuses with outliers indicate the mean of estimated x_p with 1 SD at proximal (x_p , 2.48 ± 0.59 ; r_p , 0.67 mm, range 0.11–15 mm) and peripheral arterial regions (x_p , 2.41 ± 0.40 ; r_p , 0.06 mm, range 0.01–0.10 mm). PA, pulmonary arterial tree; LPA and RPA, left and right pulmonary arterial trees, respectively; prox., proximal; peri., peripheral. r , vessel radius, presented as the mid-point and its range for the same reason as described in the legend of Figure 1; x , radius exponent, defined by in equation (1 or 3); s and p, systemic and pulmonary, respectively.

Table 5. Coupled conditions of Ω and Re in the physiological mammalian systemic artery, which render x to get close to 2.70 as predicted by the rigid model.

Ω	5	20	40	60
Re	70	300	500	800
x	2.69	2.68	2.71	2.70

Re , Reynolds number, defined by equation (31); x , radius exponent, computed by equation (32) with coupled values of Ω and Re under $\alpha = 1.0$. α and Ω represent exponent and proportional coefficients of the relationship between vessel length and radius, respectively, defined by equation (16).

where x_p of a dog (Gan and Yen 1994) and a cat (Zhuang et al. 1983) also stayed at the same level in the similar range of r_p . Stable and consistent peripheral x_p among normal humans and these mammals are probably due to similar respiratory physiology and pulmonary circulation (Table 3B).

Our estimates of α and Ω agreed with the results reported by previous studies (Suwa and Takahashi 1971; Dawson et al. 1999), as indicated in Table 4A and B. We could confirm the empirically reported relationship between r and l as written in equation (16) by large correlation coefficients (r) between $\ln r$ versus $\ln l$ (Table 4A and B). Although several estimated values of Ω differed to a considerable degree between proximal and peripheral pulmonary arteries, the difference was partly due to the much smaller number of peripheral samples in the data than proximal samples. As indicated in Tables 2 and 4, α_p actually stayed slightly below 1.0 or ~ 0.8 , which provides $x_p \approx 2.27$ (Fig. 4B) from equation (26). The range of α from 0.72 to 1.23, as indicated in Tables 2 and 4, yields x

in the elastic arterial model from 2.24 to 2.41. On the other hand, the same range of α from 0.72 to 1.23 causes only a trivial deviation of x in the rigid model (eq. 32); for example, x resulted in 2.348–2.350 ($\Omega = 1.5$; $Re = 1000$) and 2.996–2.997 ($\Omega = 50$; $Re = 4$).

Our elastic arterial model explains $x = 2.33$ by Bernoulli's effect. However, it has conventionally been explained by Uylings' theoretical prediction under the condition of *complete turbulence* in a rigid cylindrical vessel (Uylings 1977), one of the most influential theories (Sherman 1981; Horsfield and Woldenberg 1989; Huang et al. 1996; Bennett et al. 2000; Olufsen et al. 2000). But it still remains controversial to explain the radius exponent reported in proximal systemic arteries as well as in the whole pulmonary arterial tree by the presence of turbulence alone (Caro et al. 1978; Roy and Woldenberg 1982; Horsfield and Woldenberg 1989; Nichols et al. 2011). Because the peak Re in human systemic and pulmonary arteries is estimated as <2000 except for the region just above the aortic valve (Caro et al. 1978; Nichols et al. 2011), it conflicts with the presence of continuous turbulence. Horsfield and Woldenberg (1989) stated that turbulence by itself could not fully account for the coexistence of both $x_p = 2.3 \pm 0.1$ and $Re < 2000$ at the same time in the case of pulmonary arteries, while several more direct effects resulting from arterial wall elasticity should also intervene.

The result in our rigid arterial model led us to represent x with a novel function of Re and Ω , as presented in equation (32). This equation provides the general solution of optimal x under various blood flow levels, involving both Murray's and Uylings' theories. First, Murray's $\partial C/\partial r = 0$ in equation (11) is a particular solution of $\partial E/\partial r = 0$ of equations (10 and 20). The ratio of U_K over ΔU_P in equation (20) is proportional to Re when α is equal to 1.0:

Table 6. Categorization of systemic arteries by radius exponent in the two canine data sets in literature.

Locality	References	x_s	Range of radius (mm)	Expected wall property	Expected range of Reynolds number
Proximal		$x_s \sim 2.3$		Elastic	400–1100 ¹
Dog	Milnor (1982)	2.32 ± 0.06	0.65–9.5		
Dog SMA	Sherman (1981)	2.30 ± 0.16	0.5–1.5		
Intermediate		$x_s \sim 2.7$		Elastic-muscular	4 ² –400
Dog	Milnor (1982)	2.65	0.225		
Dog SMA	Sherman (1981)				
Peripheral		$x_s \sim 3.0$		Muscular (rigid)	0.1 ³ –4
Dog	Milnor (1982)	2.95	0.075		
Dog SMA	Sherman (1981)	3.10 ± 0.24^4	0.011–0.096		

x , radius exponent, defined by equation (1 or 3); s , systemic; SMA, superior mesenteric artery. Sources of data sets were table 2.3 (Milnor 1982) and table III (Sherman 1981).

¹Nichols et al. (2011); ²estimated from equation (34) and Mayrovitz and Roy (1983); ³from Kizilova (2006); ⁴does not include the rank 4 arterial data (Sherman 1981) as an outlier.

$$\frac{U_K}{\Delta U_P} = \frac{(1/2)\rho q(q/\pi r^2)^2}{8\mu\Omega r^2 q^2/\pi r^4} = \frac{vr\rho}{16\mu\Omega} \propto Re. \quad (35)$$

Because the result of $\partial E/\partial r = 0$ in equation (20) approximates that of $\partial C/\partial r = 0$ in equation (7) under the condition of $U_K \ll \Delta U_P$ and Re becomes sufficiently low as shown in equation (35), x reaches 3.00, which Murray's (1926) law eventually advocates. Moreover, Uylings' (1977) theory is another particular solution of $\partial E/\partial r = 0$ under $Re \rightarrow \infty$. E in equation (20) appears similar to equation (19) under the inverse condition of $\Delta U_P \ll U_K$, where Re rises sufficiently high as in equation (35), and x approaches 2.33, which is compatible with what Uylings' model relates. The complete turbulence in equation (20) means that blood flow closely mimics the ideal fluid with Bernoulli's principle.

However, our model does not explain the actual morphometric data of $x < 2$ or > 3 observed in some particular states of normal mammalian vasculatures (Woldenberg 1983; LaBarbera 1995; Dawson et al. 1999; Bennett et al. 2000). Furthermore, our theoretical results do not necessarily account for radius exponents found in some pathophysiological arterial remodeling processes of human and/or mammalian diseases. Ghorishi et al. (2007) reported the mean x_p to be 1.671, which is not accountable by our model, at $0.01 \leq r_p \leq 10$ mm in cast morphometry of a 2-month-old lamb with secondary pulmonary hypertension (PH) caused by surgically produced left-to-right (L–R) shunt in the fetal period. However, the same shunt lamb's x_p targeted 3.0 at the most peripheral pulmonary arterioles ($r_p \leq 0.01$ mm) in their Figure 2B (Ghorishi et al. 2007), while its x_p stayed around 2.0–2.3 at r_p from 0.4 to 3 mm. Our recent analysis of hemodynamic data revealed that the estimated x_p in patients with congenital L–R shunt defects increased gradually from 2.5 to 3.0 in peripheral pulmonary resistive arteries whose radius range was assumed to be $0.01 \leq r_p \leq 0.1$ mm in accordance with the severity of secondary PH, while x_p of controls remained at 2.2 (Nakamura et al. 2011). Congenital L–R shunt defects induce medial hypertrophy and vasoconstriction of intra-acinar arteries ($0.004 \leq r_p \leq 0.1$ mm) with secondary PH a few months after birth along the postnatal course of the disease (Michel et al. 1985; Ghorishi et al. 2007). Both of these pathophysiological changes are considered to induce strikingly decreased elasticity and increased rigidity of intra-acinar arterial wall properties.

There are limitations for this model analysis. The energy function E in this analysis did not take into account non-Newtonian effects and energy dissipations due to either turbulence or arterial ramifications. Bernoulli's equation is not necessarily guaranteed through arterial ramifications but holds true for a single elastic

artery and/or valve (Lima et al. 1983a,b; Bermejo et al. 2002). Because most morphometric studies were performed with formalin-fixed specimens or by the resin cast method, their data do not necessarily reflect actual in vivo pulsatile hemodynamic realities (Suwa and Takahashi 1971; Singhal et al. 1973; Bennett et al. 2000; Nichols et al. 2011). The concept of the optimality principle itself cannot escape some limitations. First, the in vivo vascular system must meet multiple functional requirements that are not fully expressible in terms of mathematical optimality conditions. Second, there is no guarantee that the vascular system will attain a mathematically deduced optimal state: in other words, the actual vessel structure of a living body shows significant asymmetry and heterogeneity (Woldenberg 1983; Griffith and Edwards 1990; Dawson et al. 1999; Bennett et al. 2000).

Combining a novel modification of Murray's law and a scaling exponent between vessel radius and length, our model proposes a new approach to account for the typically different hemodynamic conditions in elastic and rigid arterial models leading to the radial exponent 2.33 and continuously changing from 2.33 to 3.0 as a function of Reynolds number, respectively. They are known as Uylings' law for turbulence and Murray's law for laminar flow, respectively. In spite of the above-mentioned limitations, our model study explains the radius exponent in the elastic arterial system not by turbulence but by its elasticity and Bernoulli's effect, and our novel expression of x in rigid arteries is a step for further understanding the relationship among the fractal dimension, the situation of blood flow, and the arterial scaling structure. From the practical viewpoint, the results of theoretical approaches including ours will enable accurate estimation of blood velocity and its feasible distribution, and could be applied to pharmacodynamics in the systemic and pulmonary circulation. Equations (26 and 28) would offer a surgically preferable reconstructive design in terms of proximal arterial branching structures, and help alleviate the total cardiac work imposed and necessary to maintain sufficient blood circulation. Reflecting both the elastic and rigid arterial models in the industrial design of the artificial vascular structure would also contribute to making prostheses hemodynamically more efficient. We hope that this model analysis will eventually contribute on a theoretical basis to further biological and medical knowledge.

Acknowledgments

The corresponding author (Y. N.) thanks S. Naritaka, Y. Yogo, and Y. C. Nakamura for their continued encouragement. The authors are indebted to the anonymous reviewers of this article for his (or her) deep interest and

inspiring comments and advice. This helped us to improve and finalize the content and make findings, which otherwise might have escaped our observation.

Conflict of Interest

None declared.

References

- Al-Tinawi, A., J. A. Madden, C. A. Dawson, J. H. Linehan, D. R. Harder, and D. A. Rickaby. 1991. Distensibility of small arteries of the dog lung. *J. Appl. Physiol.* 71:1714–1722.
- Bennett, S. H., M. W. Eldridge, D. Zaghi, S. E. Zaghi, J. M. Milstein, and B. W. Goetzman. 2000. Form and function of fetal and neonatal pulmonary arterial bifurcations. *Am J Physiol Heart Circ Physiol* 279:H3047–H3057.
- Bermejo, J., J. C. Antoranz, I. G. Burwash, J. L. Rojo-Álvarez, M. Moreno, M. A. García-Fernández, et al. 2002. In-vivo analysis of the instantaneous transvalvular pressure difference-flow relationship in aortic valve stenosis: implications of unsteady fluid-dynamics for the clinical assessment of disease severity. *J. Heart Valve Dis.* 11:557–566.
- Bhattacharya, J., and N. C. Staub. 1980. Direct measurement of microvascular pressures in the isolated perfused dog lung. *Science* 210:327–328.
- Böhrer, A. 2008. One-sided and two-sided critical values for Dixon's outlier test for sample sizes up to $n = 30$. *Econ Qual Contr* 23:5–13.
- Brody, J. S., E. J. Stemmler, and A. B. DuBois. 1968. Longitudinal distribution of vascular resistance in the pulmonary arteries, capillaries, and veins. *J Clin Invest* 47:783–799.
- Caro, C. G., T. J. Pedley, R. C. Schroter, and W. A. Seed. 1978. *The mechanics of the circulation*. Oxford University Press, Oxford, U.K.
- Dawson, C. A., G. S. Krenz, K. L. Karau, S. T. Haworth, C. C. Hanger, and J. H. Linehan. 1999. Structure-function relationships in the pulmonary arterial tree. *J. Appl. Physiol.* 86:569–583.
- Fowler, N. O. 1980. *Cardiac diagnosis and treatment*, 3rd ed. JB Lippincott, Philadelphia, PA.
- Gafiychuk, V. V., and I. A. Lubashevsky. 2001. On the principles of the vascular network branching. *J. Theor. Biol.* 212:1–9.
- Gan, R. Z., and R. T. Yen. 1994. Vascular impedance analysis in dog lung with detailed morphometric and elasticity data. *J. Appl. Physiol.* 77:706–717.
- Ghorishi, Z., J. M. Milstein, F. R. Poulain, A. Moon-Grady, T. Tacy, S. H. Bennett, et al. 2007. Shear stress paradigm for perinatal fractal arterial network remodeling in lambs with pulmonary hypertension and increased pulmonary blood flow. *Am. J. Physiol. Heart Circ. Physiol.* 292:H3006–H3018.
- Gow, B. S., and M. G. Taylor. 1968. Measurement of viscoelastic properties of arteries in the living dog. *Circ. Res.* 23:111–122.
- Grasman, J., J. W. Brascamp, J. L. Van Leeuwen, and B. Van Putten. 2003. The multifractal structure of arterial trees. *J. Theor. Biol.* 220:75–82.
- Griffith, T. M., and D. H. Edwards. 1990. Basal EDRF activity helps to keep the geometrical configuration of arterial bifurcations close to the Murray optimum. *J. Theor. Biol.* 146:545–573.
- Guyton, A. C. 1991. *Pulmonary circulation; pulmonary edema; pleural fluid*. Pp. 414–421. *Textbook of medical physiology*, 8th ed. WB Saunders, Philadelphia, PA.
- Horsfield, K. 1978. Morphometry of the small pulmonary arteries in man. *Circ. Res.* 42:593–597.
- Horsfield, K., and M. J. Woldenberg. 1989. Diameters and cross-sectional areas of branches in the human pulmonary arterial tree. *Anat. Rec.* 223:245–251.
- House, S. D., and H. H. Lipowsky. 1987. Microvascular hematocrit and red cell flux in rat cremaster muscle. *Am. J. Physiol.* 252:H211–H222.
- Huang, W., R. T. Yen, M. McLaurine, and G. Bledsoe. 1996. Morphometry of the human pulmonary vasculature. *J. Appl. Physiol.* 81:2123–2133.
- Jiang, Z. L., G. S. Kassab, and Y.C. Fung. 1994. Diameter-defined Strahler system and connectivity matrix of the pulmonary arterial tree. *J. Appl. Physiol.* 76:882–892.
- Kamiya, A., and T. Takahashi. 2007. Quantitative assessments of morphological and functional properties of biological trees based on their fractal nature. *J. Appl. Physiol.* 102:2315–2323.
- Kassab, G. S., and Y. C. Fung. 1995. The pattern of coronary arteriolar bifurcations and the uniform shear hypothesis. *Ann. Biomed. Eng.* 23:13–20.
- Kizilova, N. N. 2006. Modeling of intraorgan arterial vasculature, I: steady flow at low Reynolds numbers. *Biophysics* 51:654–658.
- Kovacs, G., A. Berghold, S. Scheidl, and H. Olschewski. 2009. Pulmonary arterial pressure during rest and exercise in healthy subjects: a systematic review. *Eur. Respir. J.* 34:888–894.
- LaBarbera, M. 1995. The design of fluid transport system: a comparative perspective. Pp. 3–27 in J. A. Bevan, G. Kaley and G. M. Rubanyi, eds. *Flow-dependent regulation of vascular function*. Oxford University Press, New York, NY.
- Leary, B. M., and M. G. Taylor. 1966. Alterations with age in the viscoelastic properties of human arterial walls. *Circ. Res.* 18:278–292.
- Lima, C. O., D. J. Sahn, L. M. Valdez-Cruz, H. D. Allen, S. J. Goldberg, E. Grenadier, et al. 1983a. Prediction of the severity of left ventricular outflow tract obstruction by

- quantitative two-dimensional echocardiographic Doppler studies. *Circulation* 68:348–354.
- Lima, C. O., D. J. Sahn, L. M. Valdez-Cruz, S. J. Goldberg, J. V. Barron, H. D. Allen, et al. 1983b. Noninvasive prediction of transvalvular pressure gradient in patients with pulmonary stenosis by quantitative two-dimensional echocardiographic Doppler studies. *Circulation* 67:866–871.
- Mandelbrot, B. B., ed. 1983. *Trees and the diameter exponent*. Pp. 156–165. *The fractal geometry of nature*. Freeman, New York, NY.
- Mayrovitz, H. N., and J. Roy. 1983. Microvascular blood flow: evidence indicating a cubic dependence on arteriolar diameter. *Am. J. Physiol.* 245:H1031–H1038.
- Meyer, J. U., P. Borgström, L. Lindbom, and M. Intaglietta. 1988. Vasomotion patterns in skeletal muscle arterioles during changes in arterial pressure. *Microvasc. Res.* 35:193–203.
- Michel, R. P., T. S. Hakim, R. E. Hanson, A. R. C. Dobell, F. Keith, and D. Drinkwater. 1985. Distribution of lung vascular resistance after chronic systemic-to-pulmonary shunts. *Am. J. Physiol.* 249:H1106–H1113.
- Middleman, S. 1995. *Modeling axisymmetric flows: dynamics of films, jets, and drops*. Academic Press, San Diego, CA.
- Milnor, W. R. 1982. *Hemodynamics*. Williams & Wilkins, Baltimore, MD.
- Murray, C. D. 1926. The physiological principle of minimum work, I: the vascular system and the cost of blood volume. *Proc. Natl Acad. Sci. USA* 12:207–214.
- Nakamura, Y., S. Awa, H. Kato, Y. H. Ito, A. Kamiya, and T. Igarashi. 2011. Model combining hydrodynamics and fractal theory for analysis of in vivo peripheral pulmonary and systemic resistance of shunt cardiac defects. *J. Theor. Biol.* 287:64–73.
- Nichols, W. W., M. F. O'Rourke, and C. Vlachopoulos. 2011. *McDonald's blood flow in arteries: theoretical, experimental and clinical principles*, 6th ed. Hodder Arnold, London, U.K.
- Olufsen, M. S., C. S. Peskin, W. Y. Kim, E. M. Pedersen, A. Nadim, and J. Larsen. 2000. Numerical simulation and experimental validation of blood flow in arteries with structured-tree outflow conditions. *Ann. Biomed. Eng.* 28:1281–1299.
- Patel, D. J., D. P. Schilder, and A. J. Mallos. 1960. Mechanical properties and dimensions of the major pulmonary arteries. *J. Appl. Physiol.* 15:92–96.
- Rossitti, S., and J. Löfgren. 1993. Vascular dimensions of the cerebral arteries follow the principle of minimum work. *Stroke* 24:371–377.
- Roy, A. G., and M. J. Woldenberg. 1982. A generalization of the optimal models of arterial branching. *Bull. Math. Biol.* 44:349–360.
- Sherman, T. F. 1981. On connecting large vessels to small: the meaning of Murray's law. *J. Gen. Physiol.* 78:431–453.
- Singhal, S., R. Henderson, K. Horsfield, K. Harding, and G. Cumming. 1973. Morphometry of the human pulmonary arterial tree. *Circ. Res.* 33:190–197.
- Struijker-Boudier, H. A. J. 2009. The burden of vascular disease in diabetes and hypertension: from micro- to macrovascular disease—the “bad loop”. *Medicographia* 31:251–256.
- Suwa, N., and T. Takahashi. 1971. Morphological and morphometrical analysis of circulation in hypertension and ischemic kidney. Urban & Schwarzenberg, Munich, German.
- Uylings, H. B. M. 1977. Optimization of diameters and bifurcation angles in lung and vascular tree structures. *Bull. Math. Biol.* 39:509–520.
- West, G. B., J. H. Brown, and B. J. Enquist. 1997. A general model for the origin of allometric scaling laws in biology. *Science* 276:122–126.
- Woldenberg, M. J. 1983. Finding the optimal lengths for three branches at a junction. *J. Theor. Biol.* 104:301–318.
- Zamir, M. 2001. Fractal dimensions and multifractality in vascular branching. *J. Theor. Biol.* 212:183–190.
- Zamir, M., and N. Brown. 1982. Arterial branching in various parts of the cardiovascular system. *Am J Anat* 163:295–307.
- Zamir, M., P. Sinclair, and T. H. Wonnacott. 1992. Relation between diameter and flow in major branches of the arch of the aorta. *J. Biomech.* 25:1303–1310.
- Zhuang, F. Y., Y. C. Fung, and R. T. Yen. 1983. Analysis of blood flow in cat's lung with detailed anatomical and elasticity data. *J. Appl. Physiol.* 55:1341–1348.

Appendix

Under the condition of $\alpha = 1.0$ at the exponent in equations (16, 29) can be transformed to

$$\frac{2\rho}{(2 + \alpha)K\pi^3\Omega} \cdot \frac{q^3}{r^3} + \frac{8(4 - \alpha)\mu}{(2 + \alpha)K\pi^2} \cdot \frac{q^2}{r^2} \cong r^4. \quad (\text{A1})$$

Using a real number ε as a proportional coefficient, equation (1) can be written as

$$q = \varepsilon r^x. \quad (\text{A2})$$

When f is defined as

$$f = \frac{q}{r}. \quad (\text{A3})$$

as a method to calculate equation (A1), the equation is simplified as

$$Af^3 + Bf^2 = r^4. \quad (\text{A4})$$

$$\text{where } A = \frac{2\rho}{(2 + \alpha)K\pi^3\Omega} \text{ and } B = \frac{8(4 - \alpha)\mu}{(2 + \alpha)K\pi^2}. \quad (\text{A5})$$

To make the succeeding composite functions easier or clear-cut for differential calculus, we tentatively define g , y , and z as follows for convenience:

$$g = \ln f, \quad (\text{A6})$$

$$y = \ln(Af^3 + Bf^2), \text{ and} \quad (\text{A7})$$

$$z = \frac{\partial y}{\partial g}, \text{ respectively} \quad (\text{A8})$$

Equations (A2, A3, and A6) give us

$$g = \ln \varepsilon + (x - 1) \ln r. \quad (\text{A9})$$

Equations (A4 and A7) lead eventually to

$$y = 4 \ln r. \quad (\text{A10})$$

Eliminating r in equation (A9) by equation (A10) yields

$$g = \ln \varepsilon + (x - 1) \frac{y}{4}. \quad (\text{A11})$$

Partial differentiation of g in equation (A11) with respect to y and equation (A8) results in

$$\frac{\partial g}{\partial y} = \frac{x - 1}{4} = \frac{1}{z}. \quad (\text{A12})$$

On the other hand, equations (A6, A7, and A8) provide

$$z = \frac{\partial y}{\partial g} = \frac{dy}{df} \cdot \frac{df}{dg} = \frac{3Af^2 + 2Bf}{Af^3 + Bf^2} f = \frac{3Af + 2B}{Af + B}. \quad (\text{A13})$$

With equations (A5, A12, and A13) we can describe x as

$$x = 1 + \frac{4}{z} = 1 + \frac{4(Af + B)}{3Af + 2B} = 2 + \frac{(\rho f / \pi \mu) + 8(4 - \alpha)\Omega}{3(\rho f / \pi \mu) + 8(4 - \alpha)\Omega}.$$